Black phosphorus hybrid film enabled by covalently chemical and spatial hierarchical-locking effect for flexible supercapacitors with 100% cycling stability

Xipeng Xin,[a] Yifeng Xu,[a] Min Zhou, [a] Qingdong Liu, [a] Jingyu Fan, [a] Wei Chen, [b] Jijin Xu, [a] Jing Liu, [a] Lian Gao, [a] Kunpeng Zhao, [a] Xuefeng Song.*, [a]

[a] School of Materials Science and Engineering, Shanghai Jiao Tong University, Shanghai, 200240, China.

[b] Baosteel Roll Science &Technology Co., Ltd, Changzhou 213023, China.

E-mail address: songxfeng@sjtu.edu.cn (X.F. Song); Tel: +86-21-34203744

† Electronic supplementary information (ESI) available.

Experimental section

Synthesis of BP

Bulk BP is synthesized through a facile high-energy ball milling method. Red phosphorus (RP) powder (Alfa Aesar, 99.99%, 800 mg) and stainless steel balls (11, 10 mm in diameter; 10, 6 mm in diameter; 20, 2 mm in diameter) were put into a stainless steel vessel (50 mL) and sealed in an argon-filled glove box. The milling process was carried out with a rotation rate of 1200 rpm for 2 h using the high-energy ball milling Instrument (MSK-SFM-LN-192, Hefei Kejing Co. Ltd). This procedure is applied to transform RP into BP.

Synthesis of c-CN

Conductive c-CN material is synthesized by a "molten salt reduction denitriding" route from pristine g-C_3N_4. The pristine g-C_3N_4 is first prepared by a simple calcination method according to our previous work.[1] Then, the obtained g-C_3N_4, Mg powder, and $AlCl_3$ were homogeneously mixed and loaded in a stainless-steel autoclave and heated at 200 °C for 10h. After cooling to room temperature naturally, the collected precipitate was put in 0.1 M hydrochloric acid and stirred for several hours. Afterward, the product was washed with distilled water and ethanol until the solution was neutral. Finally, the product was dried in a vacuum at 60 °C overnight for further use.

Synthesis of BP/c-CN

BP/c-CN hybrid is synthesized by a facile ball-milling process. The as-prepared bulk BP and c-CN were mixed with a mass ratio of 20:1. The mixed powder and stainless-steel balls (10, 10 mm in diameter; 10, 6 mm in diameter; 20, 2 mm in diameter) are placed in a stainless-steel jar (50 mL) and sealed in a glovebox under Ar atmosphere. The container is mounted on a high-energy ball milling device (MSK-SFM-LN-192, Hefei Kejing Co. Ltd), followed by ball-milling for 2h at a speed of 1000 rpm.

Computational Method

The density functional theory computations were carried out by the Vienna ab initio simulation package (VASP) using the projector augmented wave (PAW) method.[2-4] The exchange-correlation potential was represented by the Perdew–Burke–Ernzerhof (PBE) functional within the generalized gradient approximation (GGA).[5] The black phosphorus (010) and graphene (001) surfaces were used to construct the BP@C heterostructure, which has good lattice matching. The cutoff energy is set to 500 eV. The structures were relaxed until the convergence tolerances of energy and force were less than 1.0×10^{-5} eV/atom and 3.0×10^{-2} eV/Å. The *k*-point sampling grid is set to 3×3×1 The vacuum layer is 15 Å. The DFT-D3 method is used to describe the van der Waals interaction.[6] And, the adsorption energy (E_{ad}) of the H atom on BP or BP@C was calculated by:

$$E_{ad} = E(\text{sub} + \text{H}) - E(\text{sub}) - 1/2E(\text{H}_2) \quad (1)$$

Where E(sub + H), E(sub), and E(H_2) are the energy of H-adsorbed BP or BP@C, BP or BP@C, and an H_2 gas molecule, respectively.

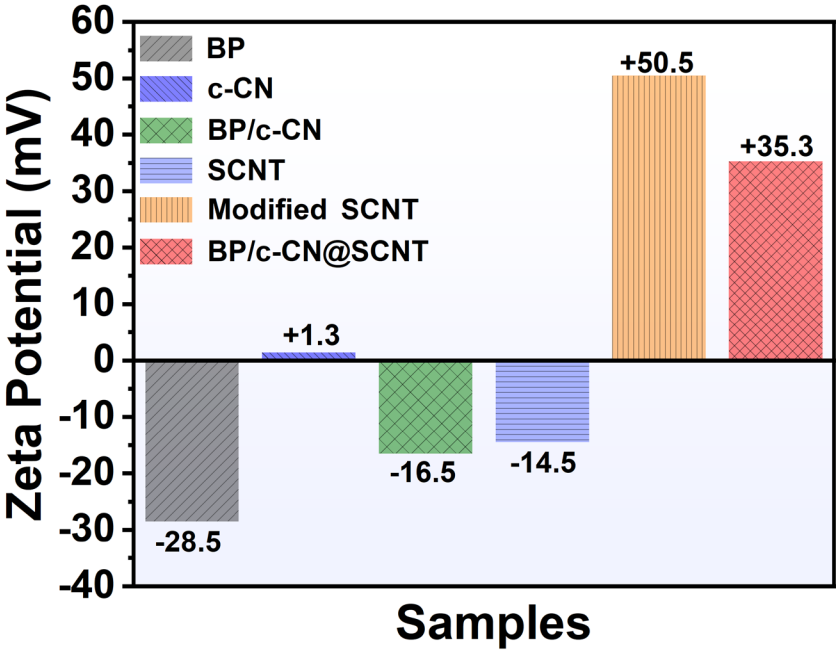

Fig. S1 Zeta potential of all samples.

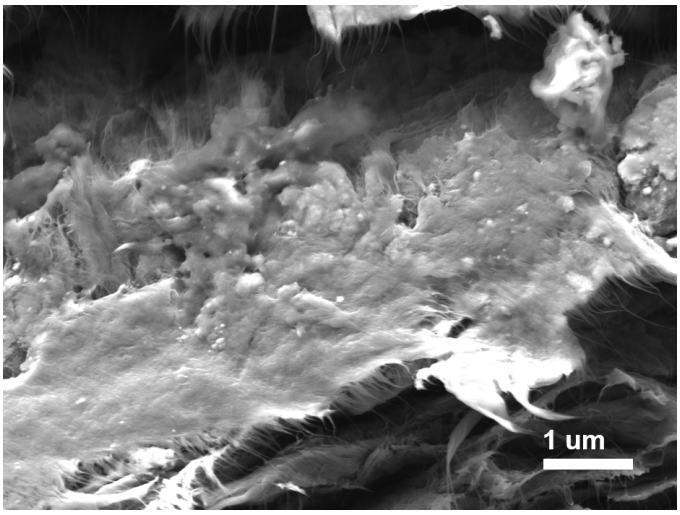

Fig. S2 The cross-section of the BP/c-CN@SCNT film.

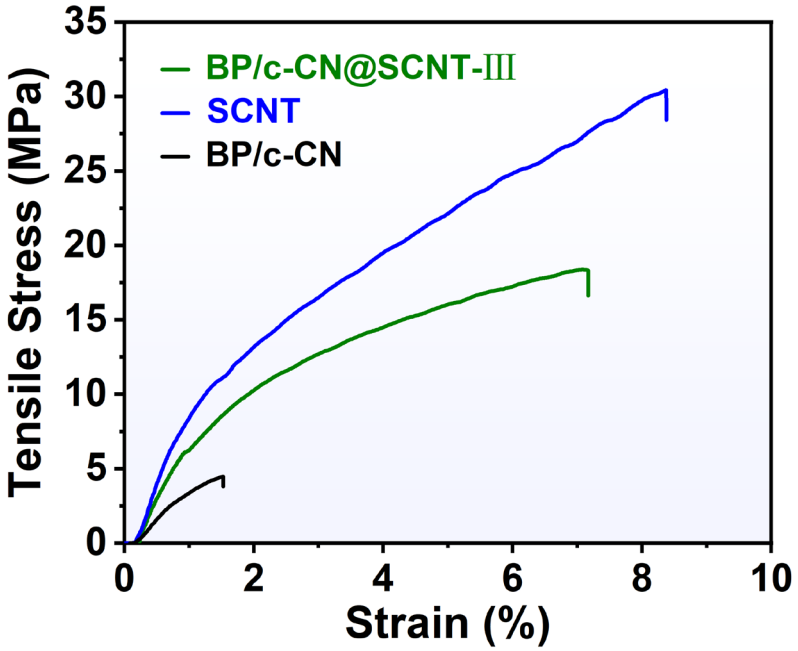

Fig. S3 Stress-strain curves of BP/c-CN, SCNT, and BP/c-CN@SCNT-III films.

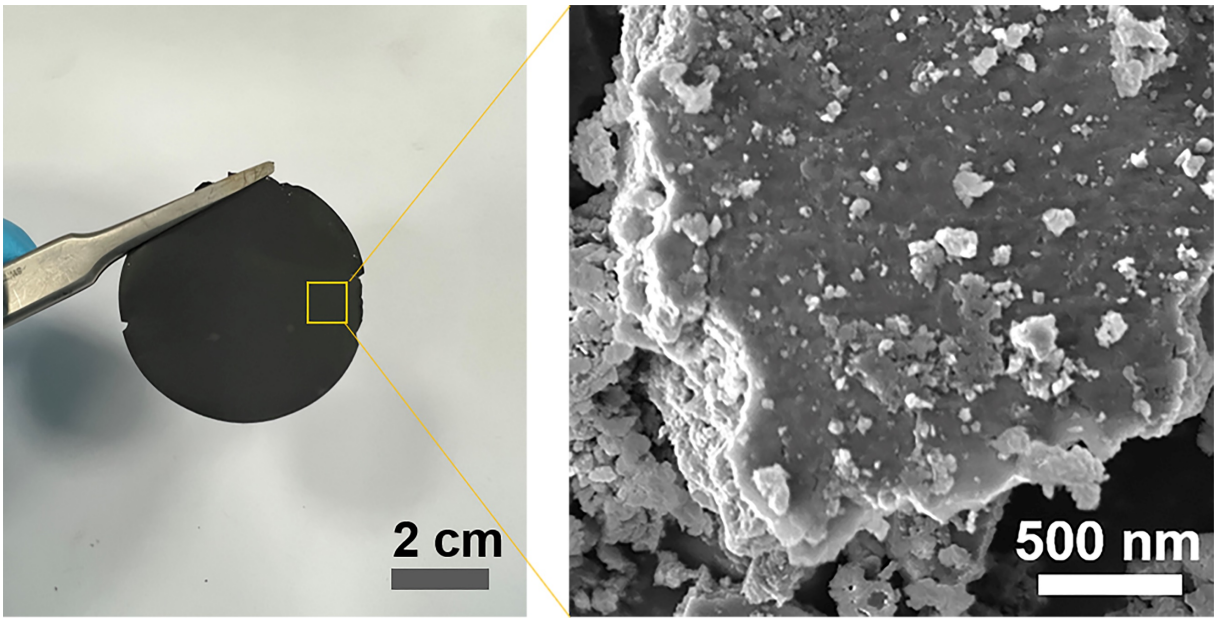

Fig. S4 Optical and SEM image of the pristine BP/c-CN film.

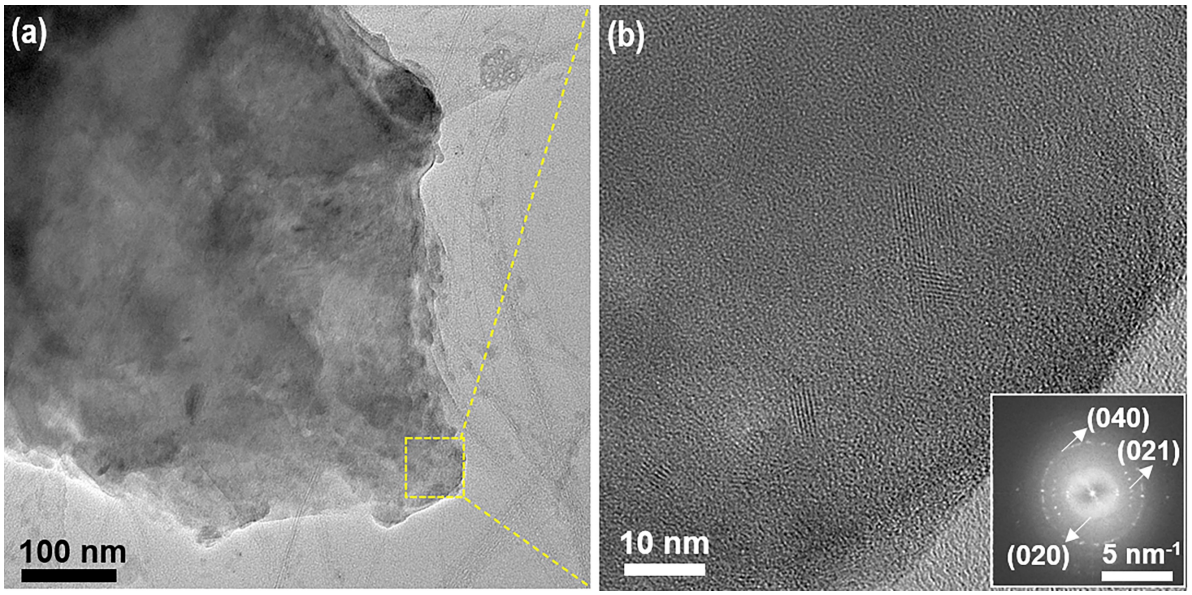

Fig. S5 (a) TEM, and (b) HRTEM images of BP/c-CN@SCNT-III sample (inset in panel b is the electron diffraction pattern).

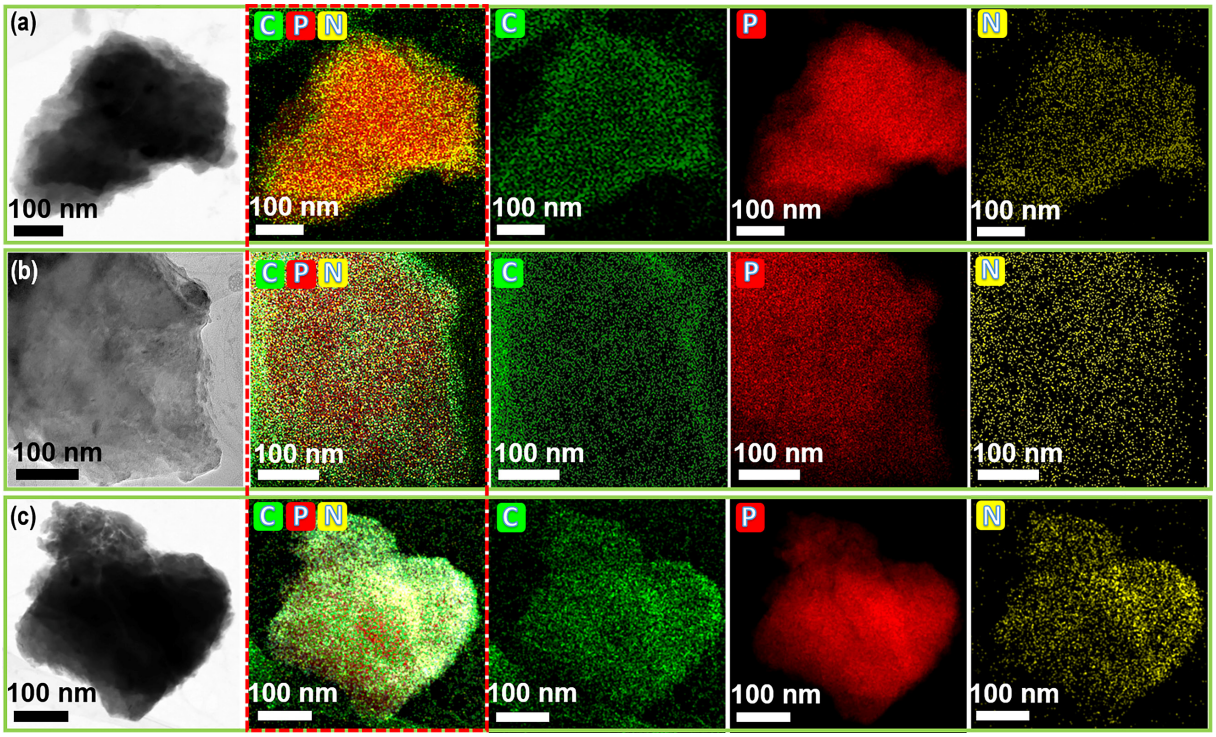

Fig. S6 EDS elemental mapping images of (a) BP/c-CN@SCNT-IV, (b) BP/c-CN@SCNT-III, and (c) BP/c-CN@SCNT-I.

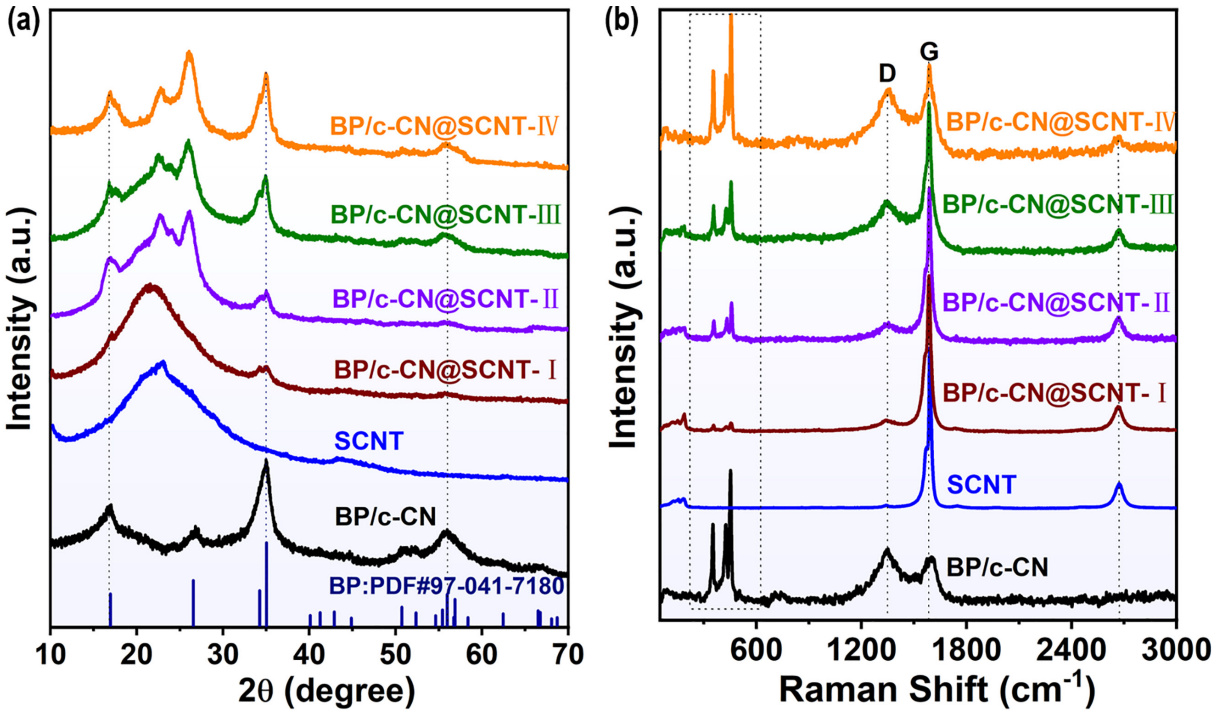

Fig. S7 (a) XRD pattern, and (b) Raman spectra of all samples.

Table S1 The thickness of the as-perpared film electrodes

Samples	**Thickness (μm)**
BP/c-CN	4.9
BP/c-CN@SCNT-IV	4.8
BP/c-CN@SCNT-I	5.5
SCNT	5.0

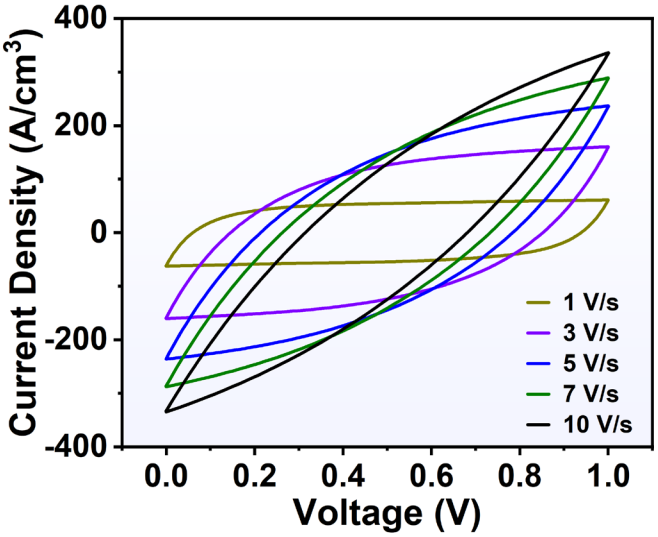

Fig. S8 CV curves at scan rates from 1 to 10 V/s of the BP/c-CN@SCNT-III film-based FSC.

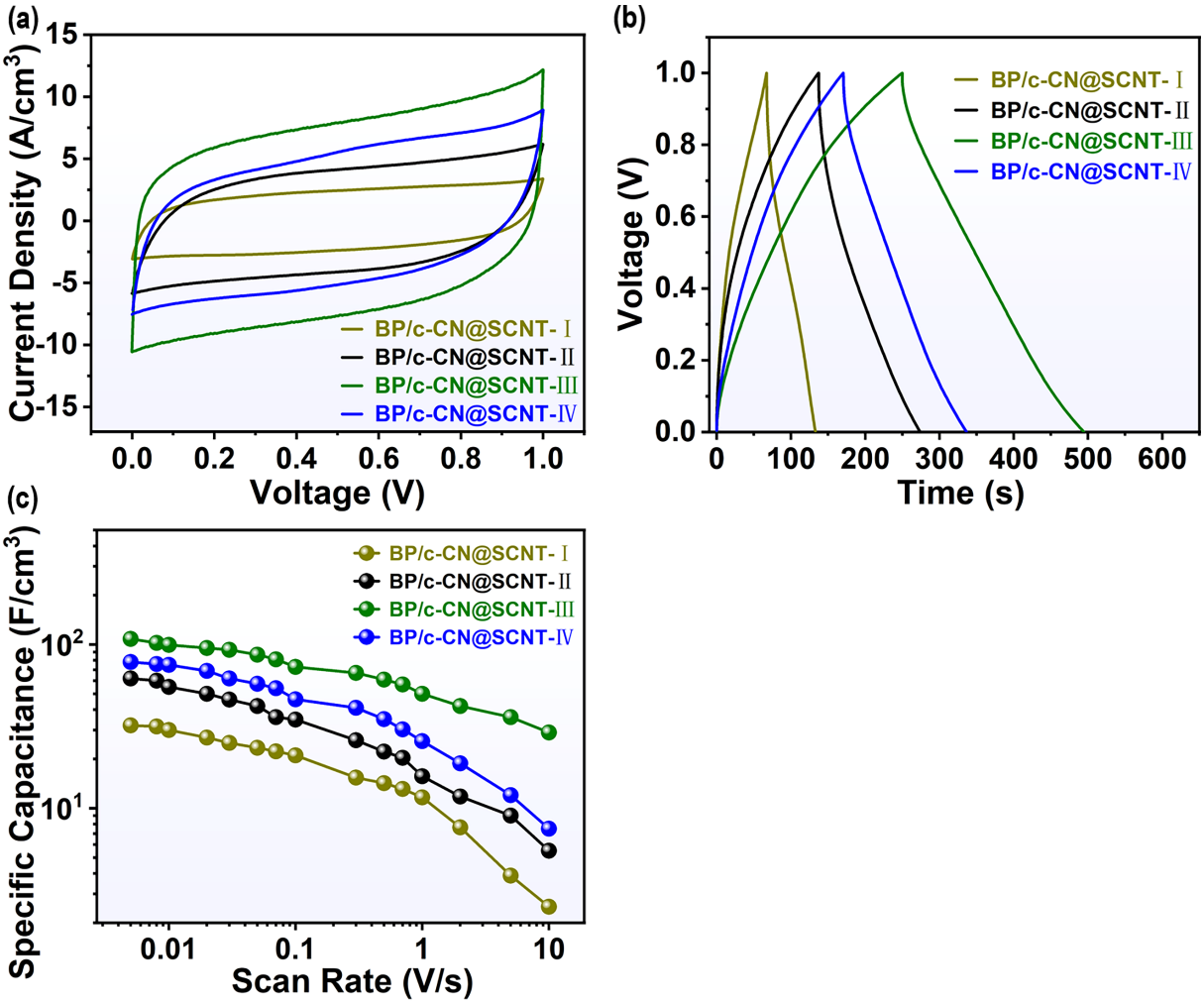

Fig. S9 (a) CV curves at the scan rate of 100 mV/s, (b) GCD curves at the current density of 0.5 A/g, and (c) The calculated specific capacitances under different scan rates of devices based on BP/c-CN@SCNT-I, BP/c-CN@SCNT-II, BP/c-CN@SCNT-III, and BP/c-CN@SCNT-IV.

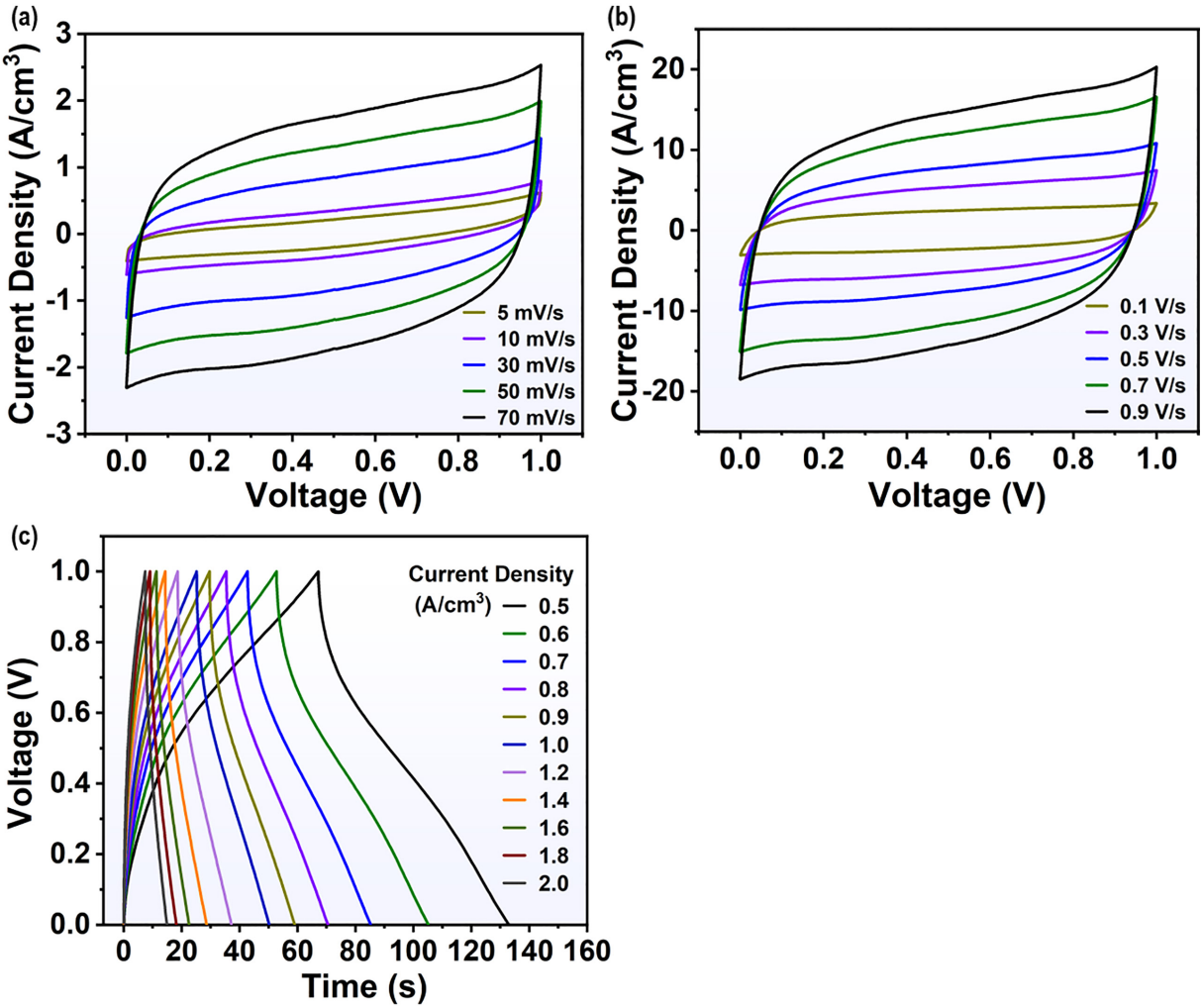

Fig. S10 (a, b) CV curves at various scan rates from 5 to 900 mV/s, and (c) GCD curves of BP/c-CN@SCNT-I film-based FSC.

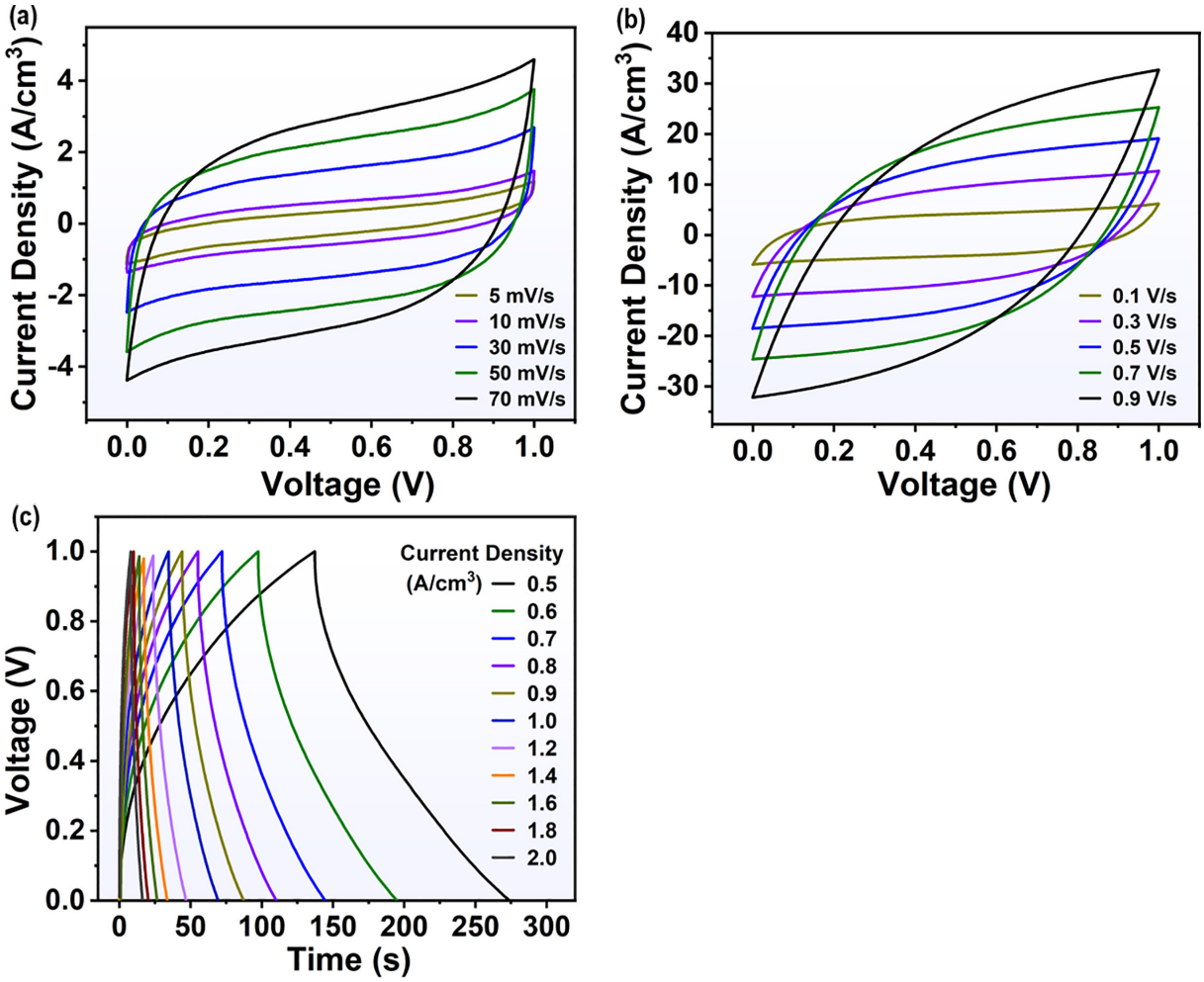

Fig. S11 (a, b) CV curves at various scan rates from 5 to 900 mV/s, and (c) GCD curves of BP/c-CN@SCNT-II film-based FSC.

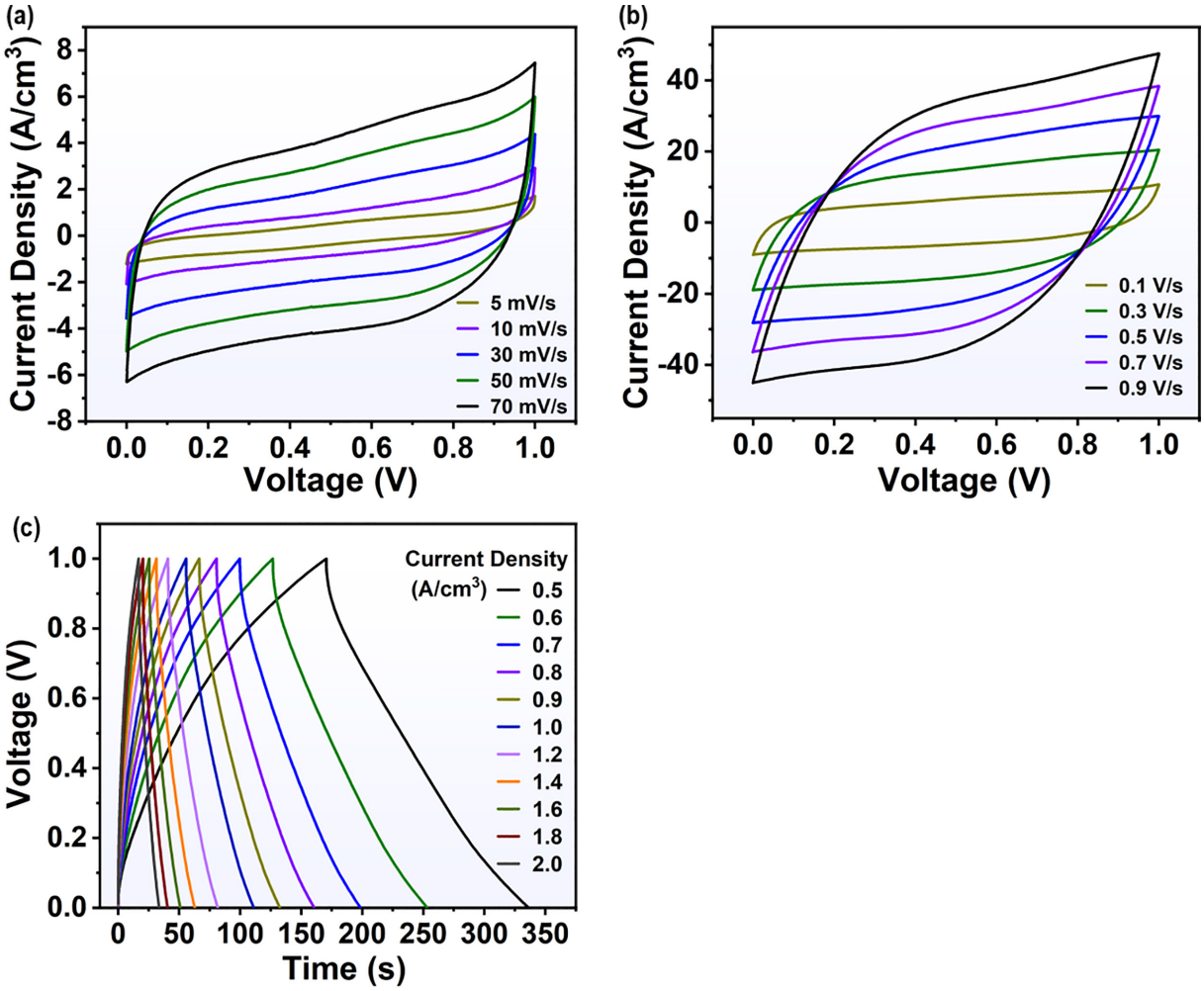

Fig. S12 (a, b) CV curves at various scan rates from 5 to 900 mV/s, and (c) GCD curves of BP/c-CN@SCNT-IV film-based FSC.

Table S2 The electrical conductivity of the samples obtained from the "four-probe method".

Samples	**Conductivity (S/m)**
BP/c-CN	32
BP/c-CN@SCNT-IV (BP/CN: SCNT=30:1)	210
BP/c-CN@SCNT-III (BP/CN: SCNT=15:1)	877
BP/c-CN@SCNT-I (BP/CN: SCNT=1:1)	1250
SCNT	2150

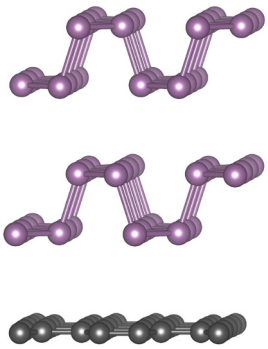

Fig. S13 The simplified configurational model of the BP@C interface.

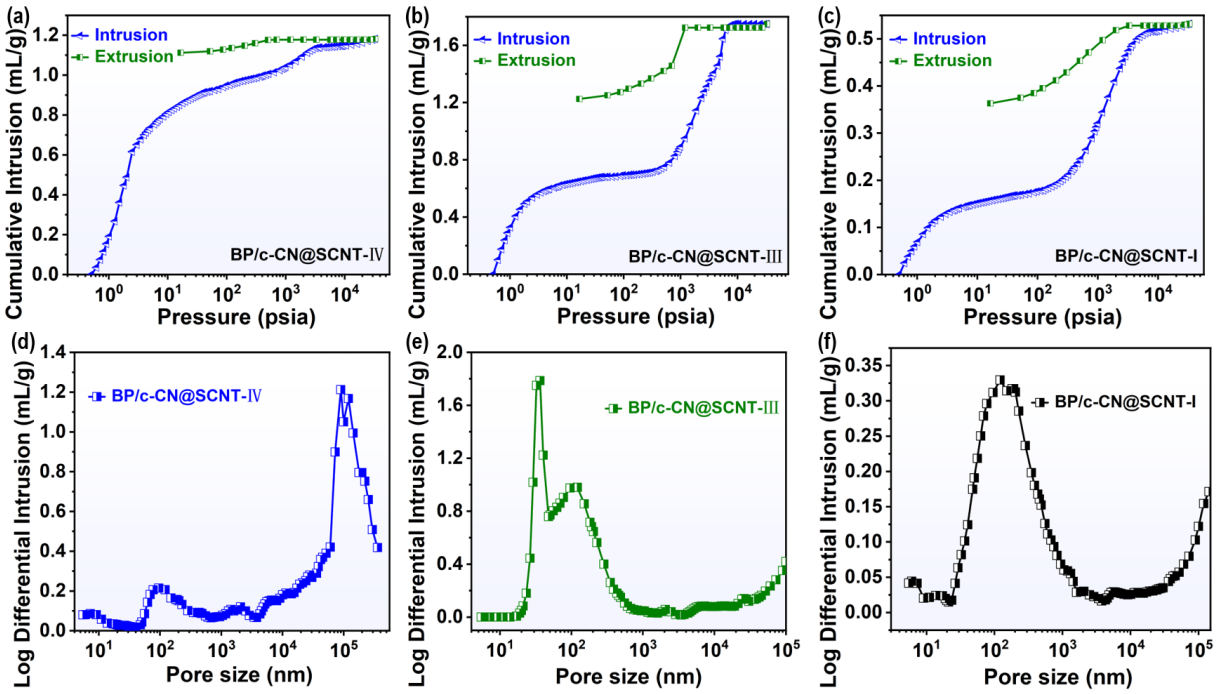

Fig. S14 (a-c) Mercury intrusion-extrusion cycles for the BP/c-CN@SCNT-IV, BP/c-CN@SCNT-III, and BP/c-CN@SCNT-I film, respectively. The pore size distributions of (d) BP/c-CN@SCNT-IV, (e) BP/c-CN@SCNT-III, and (f) BP/c-CN@SCNT-I films obtained from MICP tests.

Table S3 Structural pore parameters of BP/c-CN@SCNT-IV, BP/c-CN@SCNT-III, and BP/c-CN@SCNT-I films obtained from MICP tests.

Samples	Total pore area (m^2/g)	Total intrusion volume (mL/g)	Porosity (%)	Average pore diameter (A) (nm)
BP/c-CN@SCNT-IV	19.36	0.53	26.26	214.93
BP/c-CN@SCNT- III	**66.83**	**1.75**	**59.80**	**38.30**
BP/c-CN@SCNT- I	21.98	1.18	35.90	109.94

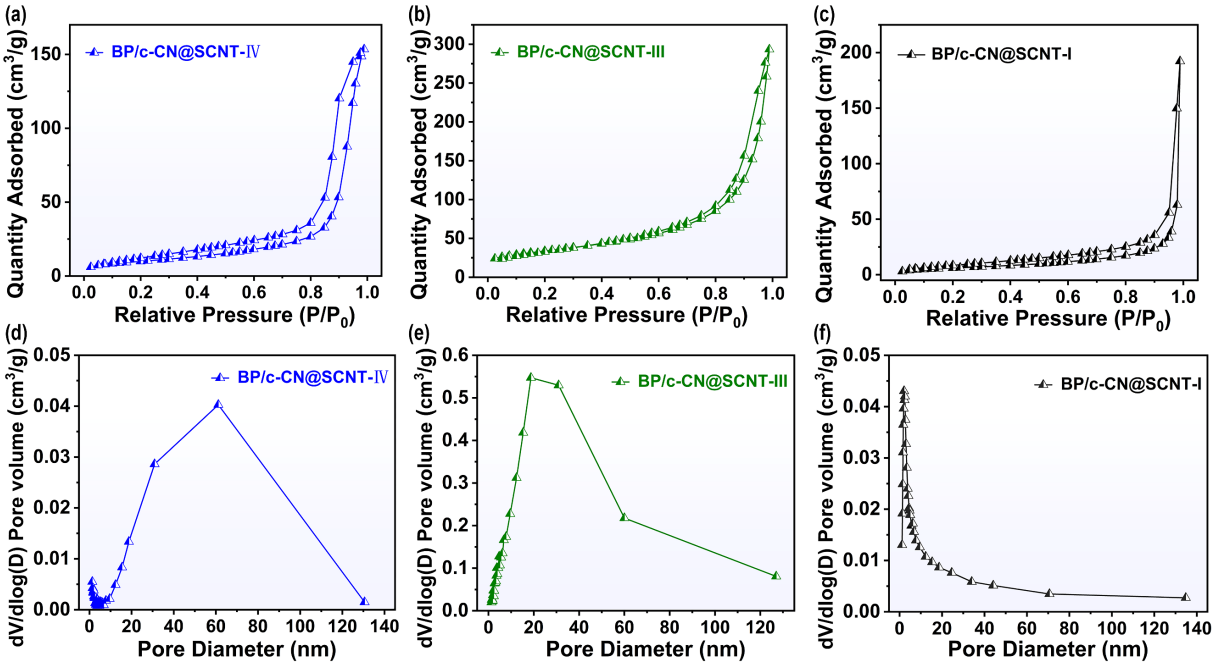

Fig. S15 (a-c) N_2 adsorption/desorption isotherms of the BP/c-CN@SCNT-IV, BP/c-CN@SCNT-III, and BP/c-CN@SCNT-I films, respectively. (d-f) The BJH pore size distribution of BP/c-CN@SCNT-IV, BP/c-CN@SCNT-III, and BP/c-CN@SCNT-I films, respectively.

Table S4 Structural pore parameters of BP/c-CN@SCNT-IV, BP/c-CN@SCNT-III, and BP/c-CN@SCNT-I films obtained from N_2 adsorption/desorption measurements.

Samples	BET surface area (m^2/g)	Pore volume (cm^3/g)	Average pore diameter (nm)
BP/c-CN@SCNT-IV	38.94	0.14	63.93
BP/c-CN@SCNT- III	**113.40**	**0.72**	**18.76**
BP/c-CN@SCNT- I	52.06	0.36	1.35

Table S5 Specific capacitance and cycling ability of our FSC compared with other BP-based supercapacitors.

Works	Material	Specific capacitance	Electrolyte	Cycle ability
This work	**BP/c-CN@SCNT**	**108 F/cm^3 at 0.005 V/s**	**PVA/H_3PO_4**	**100% after 50 000 cycles**
Ref. 8	BP Nanoflakes	14.5 F/cm^3 at 0.01 V/s	PVA/H_3PO_4	84.5% after 10 000 cycles 71.8% after 30 000 cycles
Ref. 9	BP/CNTs	41.1 F/cm^3 at 0.005 V/s	PVA/H_3PO_4	91.5% after 10 000 cycles
Ref. 11	BP/Polyaniline	354 F/g at 0.3 A/g	H_2SO_4	96% after 175 cycles
Ref. 12	BP/Polypyrrole	7.7 F/cm^3 at 0.5 A/g	PVA/H_3PO_4	99% after 10 000 cycles
Ref. 42	BP sponge	80 F/g at 0.01 V/s	PVA/H_3PO_4	80.0% after 15 000 cycles
Ref.43	CNT/MnO_2-BP	441.7 F/cm^3 at 0.01 V/s	PVA/KOH	90.5% after 10 000 cycles
Ref. 44	BP-CNTs	308.7 F cm^{-3} at 0.1 A/cm^3	$EMIMBF_4$/PVDF-HFP	90.2% after 10 000 cycles
Ref.45	BP/Mxene	896.87 F/cm^3 at 0.69 A/cm^3	PVA/H_2SO_4	91.74% after 10 000 cycles
Ref.46	BP/Mxene	361.9 F/cm^3 at 0.1 V/s	Na_2SO_4/CMC	90.9% after 40 000 cycles
Ref.47	BP/Polypyrrole	417 F/g at 0.2 A/g	EMI-TFSI	87% after 10 000 cycles

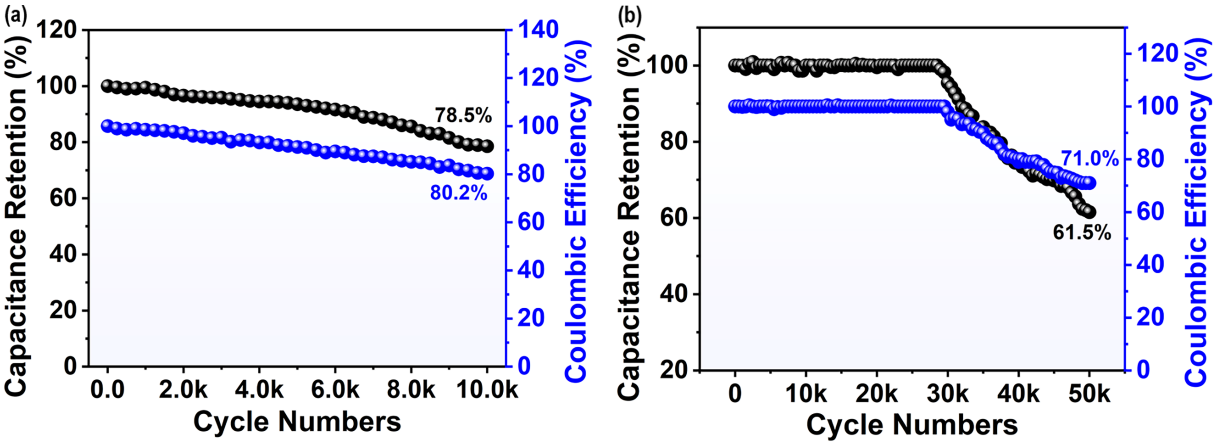

Fig. S16 Cycling stability and coulombic efficiency at a current density of 1.0 A/cm^3 for (a) BP-based FSC and (b) BP/c-CN-based FSC.

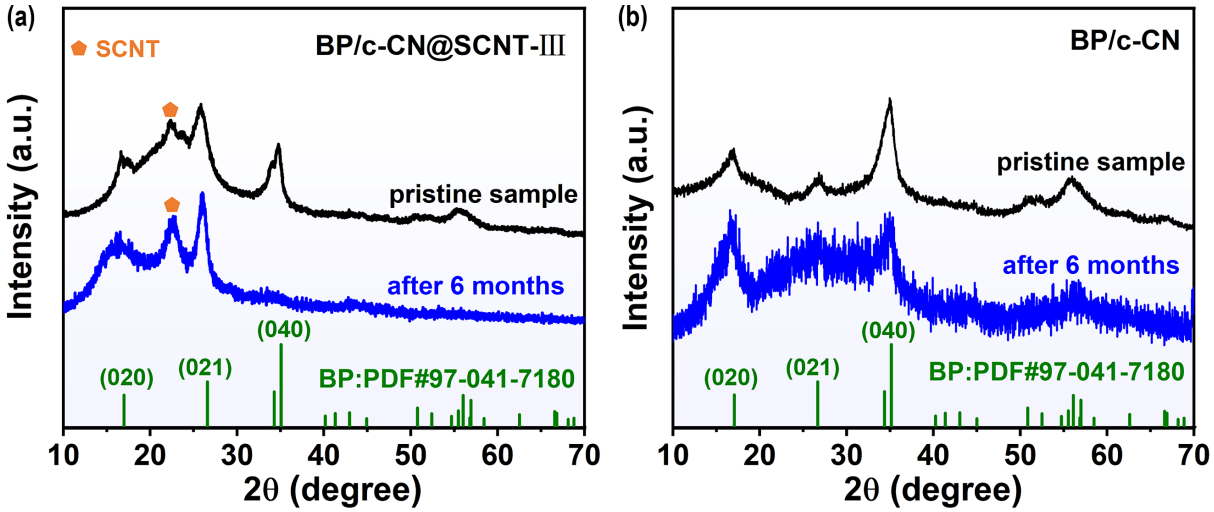

Fig. S17 XRD images of (a) BP/c-CN@SCNT-III and (b) BP/c-CN after 6 months under ambient conditions.

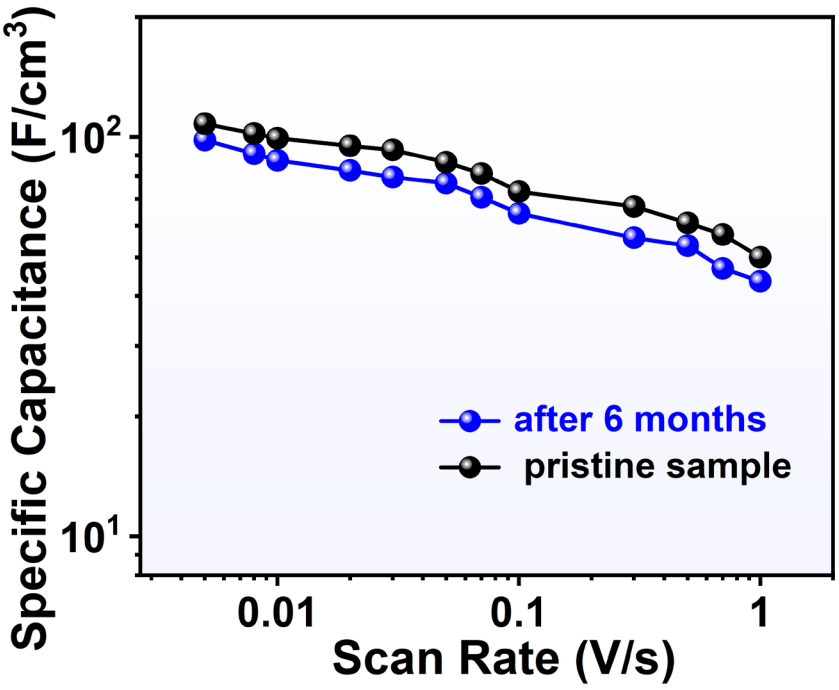

Fig. S18 Specific capacitance at various scan rates of BP/c-CN@SCNT-III after 6 months under ambient conditions.

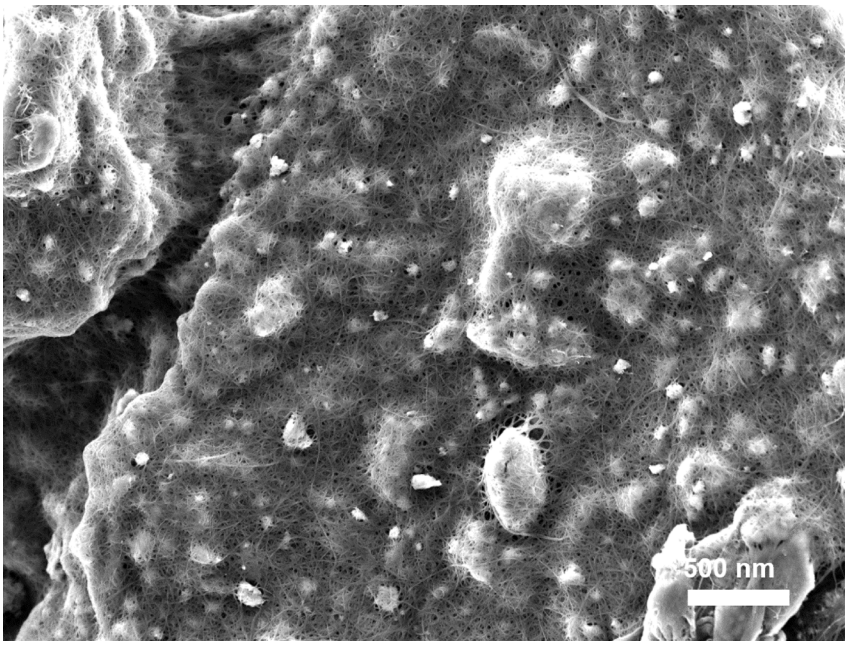

Fig. S19 SEM image of the BP/c-CN-III film after 50 000 cycling tests.

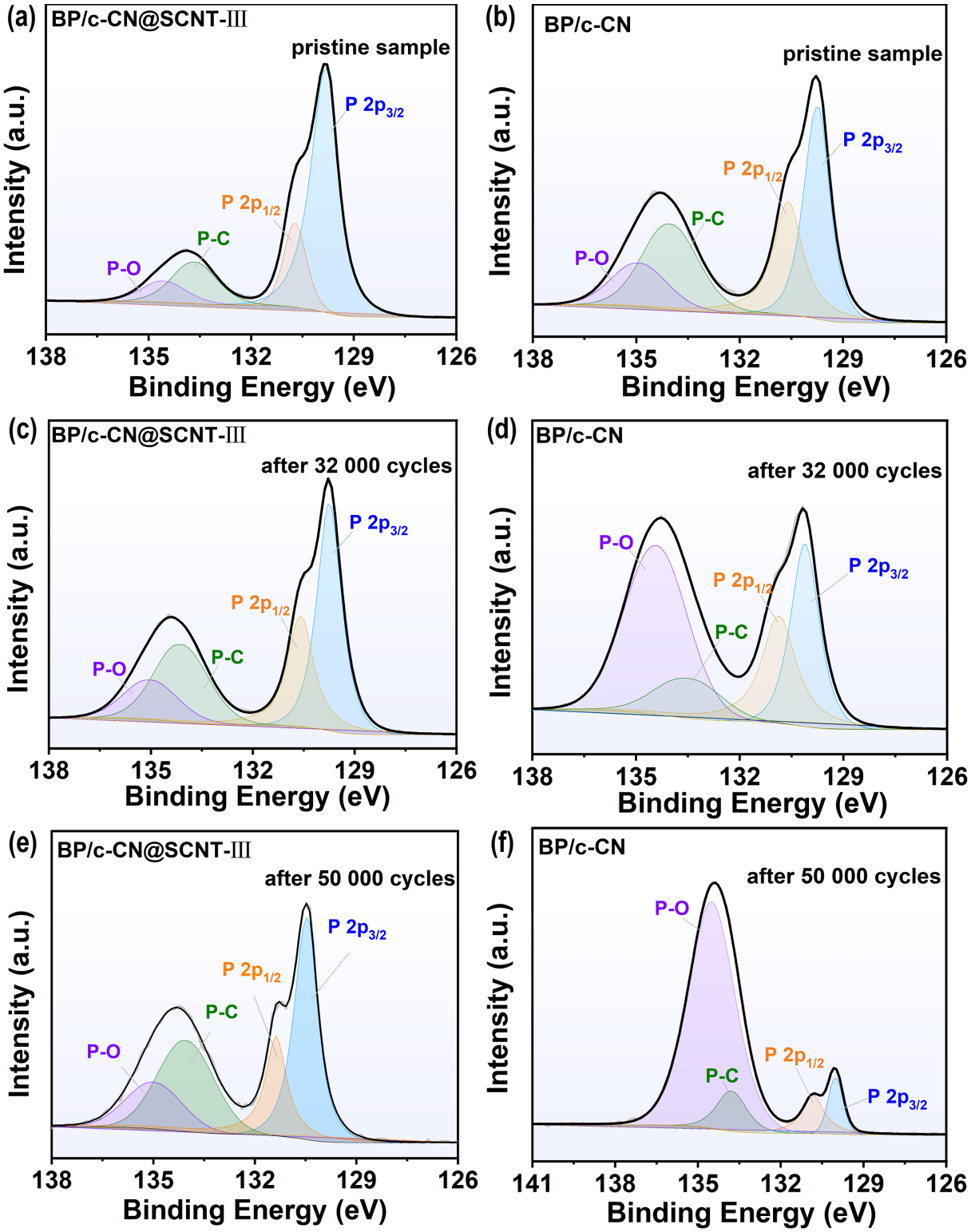

Fig. S20 High-resolution P 2p XPS spectra of (a, c, e) BP/c-CN@SCNT-III, and (b, d, f) BP/c-CN after different cycles.

Table S6. High-resolution P2p XPS analysis of BP/c-CN@SCNT-III and BP/c-CN samples after different cycles.

Sample \ Bonding type		P-C /at%	P-O /at%	$P2p_{3/2}$ /at%	$P2p_{1/2}$ /at%
BP/c-CN@SCNT-III	Pristine sample	16.5	11.6	55.9	16.0
	After 32 000 cycles	20.0	16.50	46.5	17.0
	After 50 000 cycles	21.8	17.7	44.5	16.0
BP/c-CN	Pristine sample	19.9	17.1	47.2	15.8
	After 32 000 cycles	14.9	42.7	25.1	17.3
	After 50 000 cycles	8.9	76.9	6.0	8.2

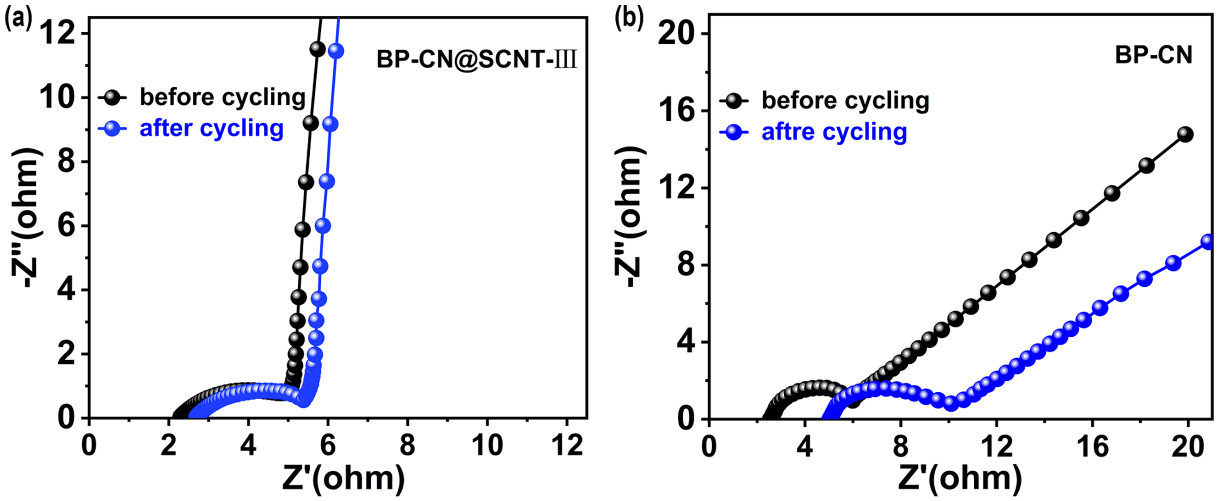

Fig. S21 Nyquist plots of (a) BP/c-CN@SCNT-III and (b) BP/c-CN film-based device before and after 50 000 cycles.

Reference

1. M. Shi, T. Wu, X. Song, J. Liu, L. Zhao, P. Zhang and L. Gao, *J. Mater. Chem. A*, 2016, **4**, 10666-10672.

2. G. Kresse and D. Joubert, *Phys. Rev. B*, 1999, **59**, 1758.

3. G. Kresse and J. Furthmüller, *Comp.Mater. Sci.*, 1996, **6**, 15-50..

4. G. Kresse and J. Furthmüller, *Phys. Rev. B*, 1996, **54**, 11169.

5. J. P. Perdew, K. Burke and M. Ernzerhof, *Phys. Rev. Lett.*, 1996, **77**, 3865.

6. K. Lee, É. D. Murray, L. Kong, B. I. Lundqvist and D. C. Langreth, *Phys. Rev. B*, 2010, **82**, 081101.